PRACH Detection Probability in the Presence of Strong Phase Noise for NR Uplink in Sub-THz Bands

Satoshi Tsuyuki
Tokyo City University
Tokyo, Japan

Yoshinobu Ota
Tokyo City University
Tokyo, Japan

Takashi Ohiwa
Tokyo City University
Tokyo, Japan

Mamoru Sawahashi
Tokyo City University
Tokyo, Japan

Satoshi Suyama
NTT DOCOMO INC.
Kanagawa, Japan

***Abstract*—This paper presents the miss detection probability (MDP) for the physical random access channel (PRACH) in the 3GPP New Radio (NR) uplink in the presence of strong phase noise (PN) in the sub-Terahertz (THz) bands. The PRACH is a physical channel that a set of user equipment (UE) first transmits in the uplink for initial access. Hence, it is needed to achieve a low PRACH MDP under a low received signal-to-noise ratio (SNR) condition. The impact of PN that is induced in local oscillators in base station and UE transceivers in the sub-THz bands is larger than that in the millimeter-wave bands. Therefore, it is important to investigate the impact of strong PN on the PRACH detection probability in the sub-THz bands. Link-level simulation results show that the Wiener PN component in a sub-THz PN model fluctuates quickly over the PRACH preamble duration. Accordingly, the strong PN in the sub-THz bands comprising the Wiener PN and uncorrelated Gaussian PN is reduced when taking the correlation over the PRACH preamble sequence duration with a 139-chip length. We show that the degradation in the PRACH MDP due to the strong PN is slight when the power spectral density (PSD) at a 0-Hz frequency offset in the Wiener PN is -25 dBc/Hz and the PSD in the Gaussian PN is lower than approximately -93 dBc/Hz.**

***Index Terms*—PRACH, phase noise, Zadoff-Chu sequence, miss detection probability, NR, sub-THz bands**

I. Introduction

In the 3GPP New Radio (NR) specifications, the physical random access channel (PRACH) is specified as a physical channel that a set of user equipment (UE) first transmits for uplink initial access [1]. PRACH formats with a short sequence are newly added to those with a long sequence in the NR specifications [1], [2]. The PRACH formats with a short sequence are applied to frequency spectra of Frequency Range 1 from 450 MHz to 6 GHz and to those of Frequency Range 2 from 24.25 GHz to 52.6 GHz [2]. They are used for a cell with small and medium cell ranges associated with a wide subcarrier spacing (SCS) such as 60 kHz and 120 kHz [1]. As a PRACH preamble sequence, a Zadoff-Chu sequence is adopted due to its advantageous features of low autocorrelation and cross-correlation [3]. In the sub-Terahertz (THz) bands, the major hardware impairments that degrade the error rate and throughput are carrier frequency offset (CFO) and phase noise (PN), which are both caused by local oscillators in an RF transceiver [5], [6]. The CFO is induced because the frequency stability of a UE local oscillator is much worse than that for the base station (BS) local oscillator. The impact of the CFO on the PRACH with a long sequence in the LTE specifications was investigated in [4]. The authors in [4] analyzed theoretically the influence of the CFO on Zadoff-Chu sequences with different cyclic shifts (CSs) based on the correlation power. However, in the initial access procedure for NR, a UE establishes a downlink access link before the UE transmits the PRACH. More specifically, a UE detects the physical layer cell ID (PCID) based on the detected primary synchronization signal (PSS) and secondary synchronization signal (SSS) sequences. Based on the detected PCID, a UE demodulates and decodes the master information block (MIB) in the physical broadcast channel (PBCH) payload. Subsequently, the UE demodulates and decodes system information block (SIB) 1 conveyed in the physical downlink shared channel (PDSCH), in which resource information of the PRACH is included. Therefore, the frequency error of a UE local oscillator is reduced to approximately 1/10 of the free-running frequency by measuring the more accurate frequency of a BS local oscillator through the downlink physical channels. Hence, a UE transmits the PRACH after pre-compensating for the CFO. Consequently, the residual CFO in the PRACH is suppressed to a low level.

In the millimeter-wave (mmW) bands, a PN model based on the Wiener random process is used commonly [7] - [9]. In [10], it was reported that the effect of the Wiener PN on the PRACH miss detection probability (MDP) is small in the mmW bands. However, [6] reported that PN is a significant impairment factor to the bit error rate or throughput in the sub-THz bands. In the sub-THz bands, the PN model comprises the Wiener PN and uncorrelated Gaussian PN [11] - [13]. Hence, it is anticipated that the effect of the PN model on the PRACH MDP in the sub-THz bands is larger than that in the mmW bands due to the high power of the uncorrelated Gaussian PN with high frequency components. However, to the best knowledge of the authors, the MDP of the NR PRACH suffering from the PN model in the sub-THz bands has not yet been reported.

This paper presents the MDP for the PRACH in the 3GPP NR specifications in the presence of strong PN in the sub-THz bands. We first investigate the PRACH MDP in the presence of the Wiener PN in the mmW bands as a reference. In the sub-THz bands, the total power of the Gaussian PN is greater

than that of the Wiener PN. Next, we investigate the effect of the Gaussian PN with high frequency components and the total PN in the sub-THz bands based on the correlation power profile at the matched filter (MF) output. Finally, we investigate the PRACH MDP in the presence of strong PN in the sub-THz bands. The reminder of the paper is organized as follows. In Section II, we describe the structure and sequences of the NR PRACH with a short sequence. Next, we detail the PRACH detection method at a BS receiver in Section III. After outlining the PN model in the sub-THz bands in Section IV, we present computer simulation results in Section V. Finally, we give our conclusions in Section VI.

II. Transmitter Structure of NR PRACH

A. Structure and Sequences of PRACH

In the NR specifications, the PRACH comprises a cyclic prefix (CP) and a preamble sequence using a Zadoff-Chu sequence [3]. Nine PRACH formats with a short 139-sequence length are specified with different CP lengths and a different repeated number of the PRACH preamble sequence [1]. Some PRACH formats include a guard period [1]. In this paper, we use PRACH Format A1. PRACH Format A1 repeats the preamble sequence N_{RP} = 2 times (N_{RP} denotes the number of repeated preamble sequences) and occupies a two-orthogonal frequency division multiplexing (OFDM)-symbol duration including the CP. In this paper, we assume the SCS of 120 kHz and 480 kHz for the mmW and sub-THz bands, respectively.

A Zadoff-Chu sequence with the sequence length of L_{RA} ($i = 0, 1, ..., L_{RA} - 1$) is represented as [3]

$$x_u(i) = e^{-j\frac{\pi ui(i+1)}{L_{RA}}}. \tag{1}$$

Here, u denotes the root index (RI). The cyclic-shifted Zadoff-Chu sequence is generated as shown in the equation below.

$$x_{u,\mu}(n) = x_u\{(n + C_\mu) \bmod L_{RA}\} \tag{2}$$

In (2), C_μ denotes the CS length. Multiple PRACH preamble sequences are generated using different RIs or different CSs. The cross-correlation of the Zadoff-Chu sequences with different CSs and with the same RI, $\gamma_{uu}(\lambda_1, \lambda_2)$, is represented as $\gamma_{uu}(\lambda_1, \lambda_2) = \frac{1}{L_{RA}} \sum_{n=0}^{L_{RA}-1} x_u(n + \lambda_1)x_u^*(n + \lambda_2) = \delta(\lambda_1 - \lambda_2)$ [4]. Here, superscript $*$ denotes the complex conjugate. The cross-correlation of the Zadoff-Chu sequences with different RIs, $\gamma_{um}(\lambda_1, \lambda_2)$, is represented as $\gamma_{um}(\lambda_1, \lambda_2) = \frac{1}{L_{RA}} \sum_{n=0}^{L_{RA}-1} x_u(n + \lambda_1)x_m^*(n + \lambda_2) = \frac{1}{\sqrt{L_{RA}}}$ [14]. Hence, the CS resource is used with high priority compared to the RI resource for generating the PRACH sequences due to almost zero cross-correlation. There is a restriction, however, that the CS length must be longer than the summation of the round trip delay time and the maximum delay time in multipath fading channels.

B. Transmitted PRACH Signal Generation

Fig. 1 shows a transmitter configuration for the PRACH signal. First, the Zadoff-Chu sequence in the time domain in (2) is converted to a frequency domain sequence using the discrete Fourier transform (DFT) as shown below [2].

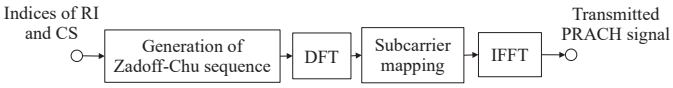

Fig. 1. Transmitter structure for PRACH signal.

$$a_{u,\mu}(k) = \sum_{n=0}^{L_{RA}-1} x_{u,\mu}(n) \times e^{-j\frac{2\pi kn}{L_{RA}}} \tag{3}$$

In (3), k denotes the subcarrier number in the frequency domain. The frequency domain PRACH sequence is mapped to the allocated subcarriers according to the designated bandwidth part (BWP), physical resource block, and subcarrier position. The UE is notified of this information using the SIB 1 bits in the PDSCH. The PRACH sequence after subcarrier mapping is converted to a time domain signal using the inverse fast Fourier transform (IFFT) as shown below [2].

$$s_{u,\mu}(t) = \sum_{k=0}^{L_{RA}-1} a_{u,\mu}(k) \times e^{j2\pi(k+Kk_1+\bar{k})\Delta f_{RA}(t-N_{CP}^{RA}T_s-t_{start}^{RA})} \tag{4}$$

In (4), variable k_1 indicates the frequency domain position of the PRACH. A detailed definition pertaining to k_1 is given in [2]. Variable K denotes the ratio of the SCS in the uplink BWP to the SCS of the PRACH, which is defined as $K = \Delta f/\Delta f_{RA}$. Here, Δf denotes 15 kHz and Δf_{RA} indicates the SCS of the PRACH. Moreover, $\bar{k}$ represents offset samples of the subcarrier position in the time domain according to the SCS. Term $N_{CP}^{RA}T_s$ denotes the CP duration, where T_s is the sample duration. Term t_{start}^{RA} denotes the starting time of the PRACH transmission, which is described in detail in [2].

III. PRACH Detection Method at BS Receiver

Fig. 2 shows the PRACH detection flow for Format A1 [15], [16]. We denote the index of two-antenna receiver diversity as h (h = 0, 1). In the subsequent simulations, we measure the MDP of one PRACH transmission, *i.e.*, we do not consider interference from other PRACHs. Ignoring the simultaneous time-aligned data channel, the received signal including the PRACH that suffers from instantaneous multipath fading is represented as $r^{(h)}(n) = \sum_{\nu=1}^{N} \xi_\nu^{(h)} D(n - \tau_\nu)e^{j2\pi n\Delta f/f_s}e^{j\theta_n} + w^{(\eta)}(n)$. Here, n denotes the sample index and $f_s = 1/T_s$ is the sampling frequency. Assuming a tapped delay line (TDL) channel model for multipath fading, ν and N are the tap index and the number of paths, respectively. Terms $\xi_\nu^{(h)}$ and τ_ν denote the channel gain and delay time of the path ν. Term $D(n)$ represents transmitted signals including the PRACH, Δf is the CFO, θ_n is PN at sample timing n, and $w^{(\eta)}(n)$ is additive white Gaussian noise with zero mean. After removing the CP in the multiplexed data channel, the BS receiver converts the received signal to a frequency domain signal as $R^{(h)}(k) = \frac{1}{\sqrt{N_{FFT}}} \sum_{n=0}^{N_{FFT}-1} r^{(h)}(n) \exp\left(-\frac{j2\pi nk}{N_{FFT}}\right)$.

Here, N_{FFT} denotes the FFT size. The PRACH is demultiplexed from the multiplexed subcarrier positions to denote the PRACH signal as $\bar{R}^{(h)}(\bar{k})$ $(0 \leq \bar{k} < 139)$. In the simulation, we assume there are 64 PRACH sequence candidates. We assume the BS receiver does not know the PRACH sequence that the target UE selected. In the simulations, we assume that the target PRACH sequence is a Zadoff-Chu sequence with the RI of $\bar{u}$ = 3 and the CS index of $\bar{\mu}$ = 0. Let $S_{u,\mu}(\bar{k})$ be the PRACH sequence in the frequency domain with RI u and CS index μ among the 64 PRACH sequence candidates. The BS MF computes the cross-correlation, $Z^{(h)}_{u,\mu}(\bar{k})$, between the received PRACH signal and each of the 64 PRACH sequence candidates in the frequency domain as shown in the equation below.

$$Z^{(h)}_{u,\mu}(\bar{k}) = \bar{R}^{(h)}(\bar{k}) \times S^{*}_{u,\mu}(\bar{k}) \tag{5}$$

After adding zeros in the subcarrier positions outside of $Z^{(h)}_{u,\mu}(\bar{k})$, the frequency domain signal is converted to a time domain signal as $z^{(h)}_{u,\mu}(n) = \frac{1}{\sqrt{N_{FFT}}} \sum_{n=0}^{N_{FFT}-1} Z^{(h)}_{u,\mu}(k) \exp\left(\frac{j2\pi nk}{N_{FFT}}\right)$. The N_{RP} = 2 correlations for the PRACH are combined in squared form. Furthermore, the correlations at the two-antenna receiver branches are combined in squared form. We set the search interval to 90% duration of the preamble sequence length from the correct received timing of the PRACH. Finally, PRACH sequence $\hat{u}$, $\hat{\mu}$, and PRACH received timing $\hat{n}$ are detected simultaneously from the combination that provides the maximum correlation power as shown below.

$$(\hat{n}, \hat{u}, \hat{\mu}) = \arg\max_{n,u,\mu} \sum_{h=0}^{1} \sum_{\eta=0}^{1} \left| z^{(h,\eta)}_{u,\mu}(n) \right|^2 \tag{6}$$

Here, term $z^{(h,\eta)}_{u,\mu}(n)$ represents the correlation of the FFT block output in the time domain of Zadoff-Chu sequence index (u, μ) at the repeated PRACH preamble sequence index, η $(\eta = 0, 1)$.

We defined the range of the correct received timing of the PRACH as $\pm T_{CD}$ with the correct PRACH received timing as the center. Term T_{CD} is represented as $T_{CD} = T_{Tol} + T_{path}$. Here, T_{Tol} denotes the time error tolerance based on the values specified in [17]. We set T_{Tol} to 70 ns and 17.5 ns for the SCS of 120 kHz and 480 kHz, respectively. Moreover, T_{path} denotes the interval in which 99% of the signal power is received according to the root mean square (rms) delay spread or scaling factor of the multipath fading channel, τ_{rms}. We set the threshold so that the PRACH false alarm probability becomes less than 0.1% [17].

IV. PN Model in Sub-THz Bands

In the mmW bands, a PN model based on the Wiener random process is used [7]. The Wiener PN sequence, $\theta = [\theta_0, ..., \theta_{K-1}]$, is represented as $\theta_k = \theta_{k-1} + \Delta_k$, where Δ_k denotes a zero mean Gaussian increment, $\Delta_k \sim \mathcal{N}(0, \sigma^2_\Delta)$ (variance σ^2_Δ denotes PN). A discrete time Wiener PN signal in the time domain is generated by passing white Gaussian noise through an infinite impulse response low-pass filter with a single pole and single zero (SPSZ) [8], [9]. In [13] and [12], a PN model was proposed for the sub-THz bands that superposes the correlated Wiener PN and the uncorrelated Gaussian PN. Accordingly, for the PN model in the sub-THz bands, we use the Wiener PN model, in which the power spectrum density (PSD) is given in the equation below [8], [9].

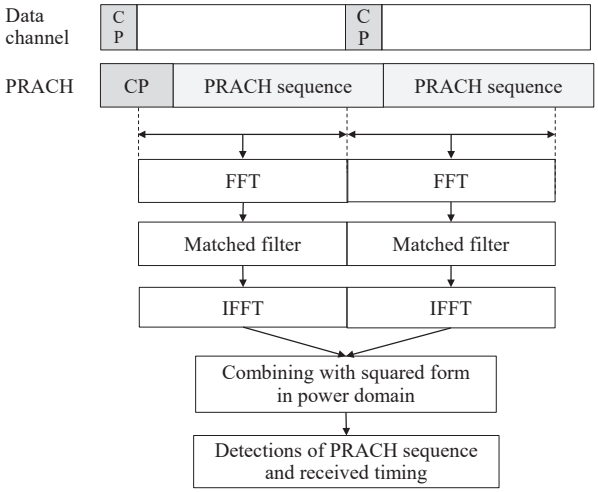

Fig. 2. PRACH detection method for Format A1.

$$S_\theta(\omega) = K^W_\theta \frac{1 + (\omega/\omega_z)^2}{1 + (\omega/\omega_p)^2} \tag{7}$$

In (7), K^W_θ is the PSD of the PN at a 0-Hz frequency offset. Here, $f_z = \omega_z/(2\pi)$ denotes zero frequency and $f_p = \omega_p/(2\pi)$ denotes pole frequencies [8]. We generate the Wiener PN using the discrete-time z transform that is derived in [9]. Meanwhile, we generate the uncorrelated Gaussian PN as $\theta^G(n) \sim \mathcal{N}(0, \sigma^2_G)$, where $\sigma^2_G = K^G_\theta B/2$ [13]. Term K^G_θ denotes the PSD of the uncorrelated Gaussian PN and B denotes the signal bandwidth. Fig. 3 shows the generated PSD of the PN model for the sub-THz bands. We set the PSD at the 0-Hz frequency offset, K^W_θ, to - 25 dBc/Hz for the Wiener PN and the PSD of the Gaussian PN in a high frequency region to K^G_θ = -100 dBc/Hz. Fig. 3 shows that the PN in the sub-THz bands is accurately generated. Although the PSD of the Gaussian PN in the high frequency region is lower than that for the Wiener PN, the total power of the Gaussian PN is greater than that for the Wiener PN.

V. Computer Simulation Results

In link-level simulations, we assume the 3GPP TDL-C channel model, in which each path suffers from independent Rayleigh fading [18]. We assume the moving speed of 3 km/h for a UE. Before we investigate the PRACH MDP in the presence of PN in the sub-THz bands, we investigate it in the presence of the Wiener PN in the mmW bands. Fig. 4 shows the in-phase component of the Wiener PN at each sample point over one OFDM symbol duration in the mmW bands. We assume the carrier frequency of f_c = 28 GHz and the SCS of 120 kHz. The FFT size is N_{FFT} = 256. In the Wiener PN model in the mmW bands, we assume f_p = 100 Hz, f_z = 7

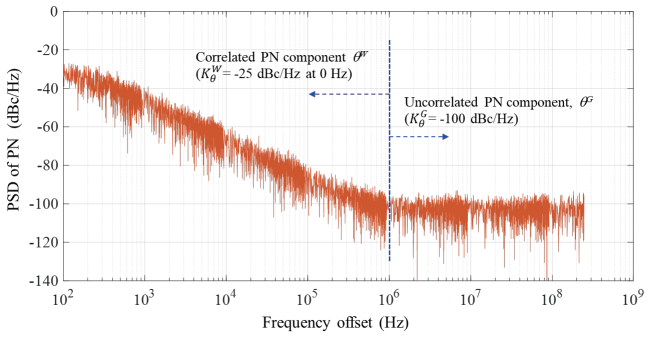

Fig. 3. PSD of PN model in sub-THz bands.

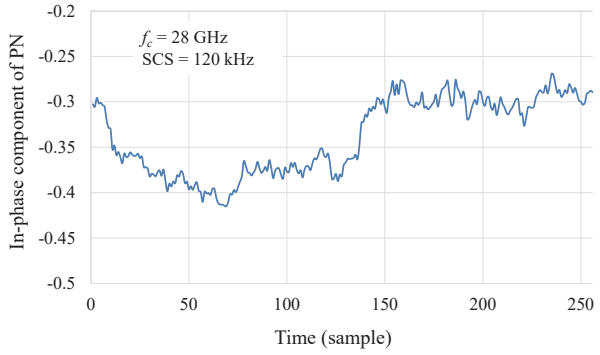

Fig. 4. Time-varying PN waveform in mmW bands.

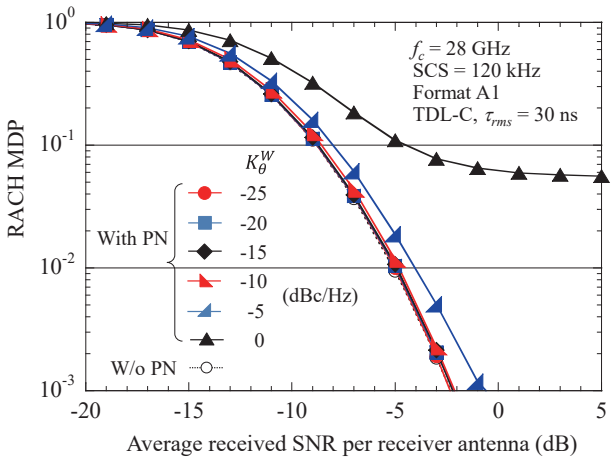

Fig. 5. PRACH MDP in the presence of PN in mmW bands.

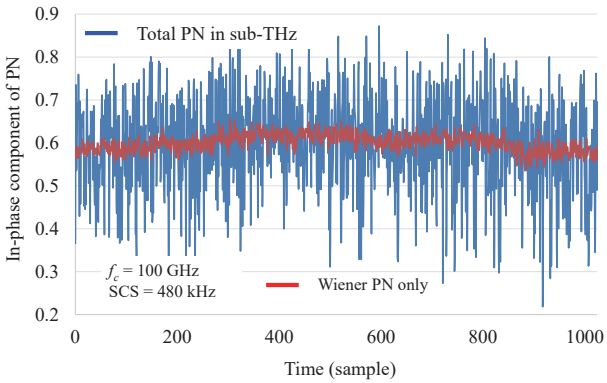

Fig. 6. Time-varying PN waveform in sub-THz bands.

MHz, and f_s = 30.72 MHz. We assume that K_θ^W at the 0-Hz frequency offset is -25 dBc/Hz. We set the τ_{rms} value in the TDL-C model to 30 ns. We do not add additive Gaussian noise. Since PRACH Format A1 is multiplexed into a two-slot duration, one OFDM symbol duration in the figure corresponds to approximately one PRACH preamble length. We see from Fig. 4 that the Wiener PN fluctuates quickly over one PRACH preamble length. Hence, we anticipate that the effect of the instantaneous time-varying Wiener PN is reduced because it is averaged over one PRACH preamble length by taking the cross-correlation with the PRACH sequence candidates.

Fig. 5 shows the MDP of PRACH Format A1 in the presence of the Wiener PN in the mmW bands as a function of the average received signal-to-noise ratio (SNR) per receiver antenna. In the figure, we parameterize the K_θ^W value. The other conditions in Fig. 5 are identical to those in Fig. 4. Fig. 5 shows that the degradation in the required average received SNR satisfying the PRACH MDP of 10^{-2} in the presence of the Wiener PN from that without PN is very slight when the K_θ^W value is lower than approximately -10 dBc/Hz. The reason for this is because the Wiener PN is averaged out when computing the correlation with the PRACH sequence candidates as shown in Fig. 4.

Fig. 6 plots the in-phase component of the time-varying PN in the sub-THz bands at each sample point over one OFDM symbol duration. We assume f_c = 100 GHz, SCS = 480 kHz, and N_{FFT} = 1024. In the Wiener PN model in the sub-THz bands, we assume f_p = 100 Hz, f_z = 10 MHz, and f_s = 491.52 MHz. We set the K_θ^W value to -25 dBc/Hz and the K_θ^G value to -100 dBc/Hz. We set the τ_{rms} value to 10 ns. We also consider the Wiener PN component only in the sub-THz PN for comparison. From Fig. 6, the PN varies quickly sample-by-sample in one PRACH preamble duration. We also see that the power of the Gaussian PN component is higher than that of the Wiener PN component in the case of K_θ^G = -100 dBc/Hz. We see that the PN including Gaussian PN in the sub-THz bands is to be averaged out when computing the cross-correlation in the MF over one PRACH preamble sequence duration.

Fig. 7 shows the correlation power profile at the IFFT output in the search interval in the presence of strong PN in the sub-THz bands. We set the K_θ^G values to -100 dBc/Hz, -95 dBc/Hz, and -90 dBc/Hz. The other conditions are the same as those in Fig. 6. In the figure, we also show the correlation power profile in the presence of the correlated Wiener PN component only in the sub-THz band PN model. Fig. 7 shows that the peak power at the correct received timing of the PRACH sequence is reduced by approximately 100%, 96%, and 83% compared to the case with only the Wiener PN when the K_G^θ value is -100 dBc/Hz, -95 dBc/Hz, and -90 dBc/Hz, respectively. However, even with the strong Gaussian PN of

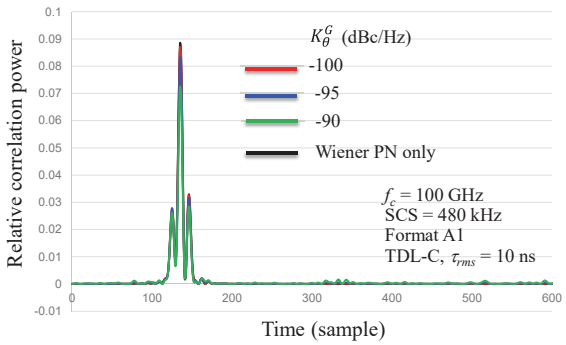

Fig. 7. Correlation power of PRACH preamble sequence in the presence of strong PN in sub-THz bands.

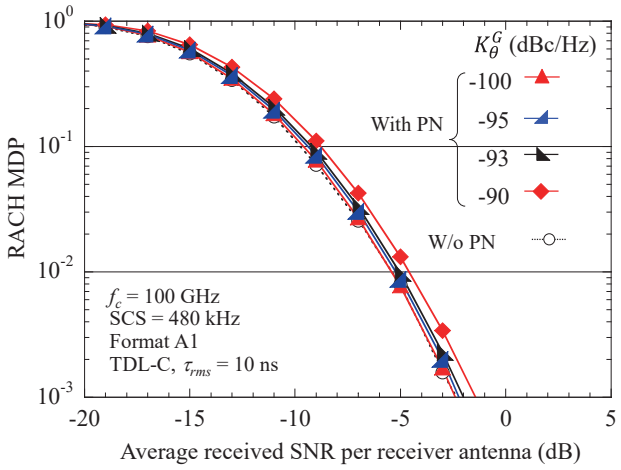

Fig. 8. PRACH MDP in the presence of strong PN in sub-THz bands.

K_G^θ = -90 dBc/Hz, high correlation power is obtained at the correct PRACH received timing. These results suggest that the correlation processing between the received PRACH signal and the PRACH sequence candidates is robust for the time-varying PN in the sub-THz bands.

Finally, Fig. 8 shows the PRACH MDP in the presence of strong PN in the sub-THz bands as a function of the average received SNR per receiver antenna. In the figure, we set K_θ^W = -25 dBc/Hz. We parameterize the PSD of the uncorrelated Gaussian PN, K_θ^G. Fig. 8 shows that the loss in the required average received SNR satisfying the PRACH MDP of 10^{-2} in the presence of strong PN in the sub-THz bands from that without PN is very slight for the K_θ^G value of lower than approximately -93 dBc/Hz. Even with K_θ^G = -90 dBc/Hz, the loss in the required average received SNR satisfying the PRACH MDP of 10^{-2} is only approximately 1 dB. Therefore, we confirm that a low PRACH MDP is achieved in the presence of strong PN in the sub-THz bands in multipath Rayleigh fading channels.

VI. Conclusion

This paper presented the PRACH MDP for the 3GPP NR specifications in the presence of strong PN in the sub-THz bands. Link-level simulation results showed that the Wiener PN component in the sub-THz PN model fluctuates with high frequency over one PRACH preamble duration. We also showed that the total power of the uncorrelated Gaussian PN component is greater than that of the Wiener PN component due to the available wide transmission bandwidth in the sub-THz bands. Accordingly, the loss in the required average received SNR satisfying the PRACH MDP of 10^{-2} in the presence of strong PN in the sub-THz bands from that without PN is negligible when the PSD of the Gaussian PN, K_θ^G, is lower than approximately -93 dBc/Hz. In conclusion, we showed that the effect of strong PN in the sub-THz bands on the PRACH MDP is slight in multipath Rayleigh fading channels.

Acknowledgment

This research and development work was supported by MIC/SCOPE #JP225003003.

References

[1] 3GPP TS 38.211, "NR; Physical channels and modulation, V16.7.0, Sept. 2021.
[2] C. Johnson, 5G New Radio in Bullets, 2019.
[3] D. C. Chu, "Polyphase codes with good periodic correlation properties," IEEE Trans. Inform. Theory, vol. IT-18, pp. 531 - 532, July 1972.
[4] M. Hua *et al.*, "Analysis of the frequency offset effect on random access signals," IEEE Trans. on Commun., vol. 61, no. 11, pp. 4728 - 4740, Nov. 2013.
[5] J.-B. Dore, Y. Corre, S. Bicais, J. Palicot, E. Faussurier, D. Ktenas, and F. Bader, "Above-90GHz spectrum and single-carrier waveform as enablers for efficient Tbit/s wireless communications," Proc. 2018 25th International Conference on Telecommunications (ICT), June 2018.
[6] M. Sarajlic *et al.*, "Waveforms for sub-THz 6G: Design guidelines," Proc. 2023 Joint European Conference on Networks and Communications & 6G Summit (EuCNC/6G Summit), June 2023.
[7] N. J. Kasdin, "Discrete simulation of colored noise and stochastic processes and $1/f^\alpha$ power law noise generation," Proceedings of the IEEE, vol. 83, no. 5, pp. 802 - 827, May 1995.
[8] C.-S. Choi, Y. Shoji, H. Harada, R. Funada, S. Kato, K. Maruhashi, I. Toyoda, and K. Takahashi, "RF impairment models for 60GHz-band SYS/PHY simulation," IEEE document 802.15-06-0477-01-003c, Nov. 2006.
[9] N. Kamiya and E. Sasaki, "Pilot-symbol assisted and code-aided phase error estimation for high-order QAM transmission," IEEE Trans. on Commun., vol. 61, no. 10, pp. 4369-4380, Oct. 2013.
[10] 3GPP TSG RAN WG1 #103 R1-2009062, "Performance evaluations and required changes on NR from 52.6GHz to 71GHz," NTT DOCOMO INC. Oct. 26 - Nov. 13, 2020.
[11] M. R. Khanzadi, D. Kuylenstierna, A. Panahi, T. Eriksson, and H. Zirath, "Calculation of the performance of communication systems from measured oscillator phase noise," IEEE Trans. on Circuits and Systems I, vol. 61, no. 5, pp. 1553 - 1565, May 2014.
[12] S. Bicais and J.-B. Dore, "Phase noise model selection for sub-THz communications," Proc. IEEE Globecom 2019, Dec. 2019.
[13] P. Neshaastegaran and M. Jian, "On the effect of oscillator phase noise on the performance of OFDM systems in sub-THz band," Proc. ICSPCS 2020, Dec. 2020.
[14] B. M. Popovic, "Generalized chirp-like polyphase sequences with optimum correlation properties," IEEE Trans. on Inf. Theory., vol. 38, no. 4, pp. 1406-1409, July 1992.
[15] 3GPP TSG-RAN WG1 #89AH R1-1711146, "PRACH preamble design for capacity enhancement," Qualcomm Incorporated, June 2017.
[16] A. Chakrapani, "On the design details of SS/PBCH, signal generation and PRACH in 5G-NR," IEEE Access, vol. 8, pp. 136617 - 136637, July 2020.
[17] 3GPP TS 38.104, "NR; Base Station (BS) radio transmission and reception (Release 16)," V16.9.0, Sept. 2021.
[18] 3GPP TR 38.901 (V14.3.0), "Study on channel model for frequencies from 0.5 to 100 GHz," Dec. 2017.